



The impact of baffle orientation on the performance of the hollow fiber membrane distillation

Abdel Nasser Mabrouk^{a,b,*}, Yasser Elhenawy^c, Mohamed Abdelkader^c, Mohamed Shatat^c

^aQatar Environment and energy Research Institute, HBKU, Qatar Foundation, Qatar, email: aaboukhlewa@qf.org.qa

^bFaculty of Petroleum & Mining Engineering, Suez University, Egypt, email: aaboukhlewa@qf.org.qa

^cFaculty of Engineering, Port Said University, Egypt, email: dr_yasser@eng.psu.edu.eg (Elhenawy), mbeshary@hotmail.com (Abdelkader), mshatat@hotmail.com (Shatat)

Received 8 January 2016; Accepted 13 June 2016

ABSTRACT

In this work, a new design of baffle is suggested in order to investigate the potential enhancement of mass and heat transfer fluxes in a hollow fiber membrane distillation module using Computational Fluid Dynamic (CFD) analysis. The number of baffle, gap height and the packing density are investigated in order to maintain the trade-off between the enhancement of mass flux and the pressure drop increase across baffles. The CFD simulation is performed in order to predict local mass fluxes, the temperature polarization coefficient (TPC), as well as the thermal efficiency of the hollow fiber membrane distillation at different design parameters. The CFD simulation results showed that the membrane module of 1.25-diameter pitch (50% packing density), eight baffle supports per unit length and at 0.075 mm gap is a good compromise between performance enhancement and pressure drop across baffles. The numerical results indicated that by adding baffles to hollow fiber membrane distillation, the mass flux is enhanced by 25% higher than that of the original module design. This is due to a reduction in thermal boundary layer resistance and increase in mass-transfer coefficient of the membrane distillation. The TPC of the module with a baffle is 16% higher than that of the module without a baffle. This increase is mainly due to the presence of turbulence flow as a result of improved hydrodynamic process. Accordingly, the thermal efficiency also increases by 16% due to enhancement made in both mass flux and TPC. However, the downside of adding baffles is relatively higher pumping power in the order of 20% higher than traditional module.

Keywords: Membrane distillation; Heat transfer; Temperature polarization; Desalination

1. Introduction

Membrane distillation is emerging technology that requires low-grade energy consumption compared with other technologies such as multi stage flash (MSF) or reverse osmosis (RO). The membrane distillation technology in desalination processes provides continuous vapor separation and can be modular and flexible for scale up. A review into membrane distillation process types has been illustrated elsewhere [1–3] which include four configurations: direct contact

membrane distillation (DCMD), air gap membrane distillation (AGMD), vacuum membrane distillation (VMD) and sweeping gas membrane distillation (SGMD).

The performance of a hollow fiber bundle most commonly is predicted assuming all fibers possess identical geometry and transport properties. Additionally, the lumen and shell flow rates are assumed to be identical for each fiber. The bundle performance is determined by calculating the performance of single fiber. By knowing the boundary layer resistance, the mass and heat balances of the feed and permeates streams can be reduced to a set of ordinary differential equations in co-current or countercurrent contacting.

* Corresponding author.

The two-dimensional (2D) conservation equations within a domain surrounding a single fiber can be solved using Computational Fluid Dynamic (CFD) tool [4]. The CFD analysis is beneficial to visualizing the flow field (including velocity, pressure, temperature and concentration) at any location in a defined flow field. The CFD simulations involving Navier–Stokes equations have been employed to provide more reliable and comprehensive information on flow fields [4–6].

CFD simulation of single-fiber hollow fiber module without and with annular baffles attached to the shell wall was performed and presented in [7]. The temperature polarization coefficient (TPC) decreases significantly with increasing mass-transfer coefficient of the membrane (C) value regardless of the existence of baffles. An improvement in TPC is reported with the presence of baffles. However, the process design of fiber bundle arrangement with baffle into vessel has not addressed yet. Additionally, the effect of various gap spaces around fiber along fiber on the hydraulic energy consumption has not addressed yet. CFD simulations to investigate the effectiveness of different promoter enhancers in single fiber DCMD module are presented in [8]. The simulation results showed that the combined annular baffle and floating spacers has a significant improvement in the heat transfer coefficient; however, the hydraulic energy is comparatively high. The configuration with appropriate floating spacer and without baffle shows is a good compromise for achieving and enhanced permeation flux with rather low pumping power. Yet, the baffles and floating spacer configuration for multi-fiber and bundle of fibers arrangement are needed to be addressed and evaluated.

Flux enhancement effects of different hollow fiber membrane module designs with baffles, spacers and modified hollow fiber geometries were experimentally investigated [9]. The results showed that the window-baffled and helical-baffled modules enhance the heat transfer coefficient by 20% and 28%, respectively. Twisted and braided module led to flux enhancement by 36% without inserting any external turbulent promoter.

The effect of spacer orientation and filament spacing on shear stress distribution and temperature polarization in DCMD modules has been studied using CFD analysis [10]. In this work, the spacer filled channel was contained a large number of cells; however, the flow becomes fully developed after passing the first few cells. The feed and distillate flow directions were countercurrent, and the inlet velocities were set equal to 5 m/s. The CFD simulation results indicated that when the spacer filaments are in direct contact with the membrane surface, stagnant zones are created and the temperature polarization is reduced. On the other hand, when the spacer filaments do not touch the membrane, a high velocity zone at the membrane surface improves shear stress as well as the heat transfer rate [10]. Experimental evaluation of using different type of baffles with hollow fiber showed that spacer-knitted module has the best performance and the mass flux improvement is significant in the laminar region. The temperature polarization effect phenomenon can be mitigated by the module with curly fibers [11].

The 2D model in DCMD under laminar flow conditions had been studied [12]. The CFD model is experimentally verified using a single-fiber module, which contained only one

straight fiber. In this lab-scale membrane distillation module, the PVFD hollow fiber membrane is assembled into Teflon housing. The hot salt feed (3.5% NaCl) is circulated in the shell while permeate water (pure) is passed through the fiber. Analysis of heat and mass transfer indicated that the hydrodynamics in the feed side might have an important role in improving membrane distillation performance.

Significant efforts have been devoted to include the baffles which extend radially in the shell in order to improve mass transfer and improve flow uniformity in the shell region as well [13,14]. Also, an adequate number of works have used the promoter enhancer using either baffles or spacers in order to suppress the temperature polarization in membrane distillation process. However, investigating whether baffles or spacers are suitable for commercial size module and investigating the effect of its geometry are rarely addressed. The aim of this work is to evaluate a new annular baffle configuration proposed for bundle of hollow fiber membranes enclosed in pressure vessel. The baffle is designed to be used as promoter enhancer, to support fibers with shell, and additionally to prevent fiber clustering due to hydrophobicity. Development of 2D CFD model in order to investigate the effect of the gap clearance, the number of baffles, and packing density will be presented. Investigating the trade-off between improved membrane distillation performance and hydraulic energy consumption is presented.

2. Mathematical model approach

2.1. Module description

Fig. 1 shows 3D drawing of the bundle of hollow fibers membrane which is assembled within baffles. The module arrangement is similar of shell and tube heat exchanger in which the bundle ends are embedded in tube sheet. The space between two tube-support there are baffles. The tube sheet is created to allow separate fluid communication with the fiber interior (lumens) and exterior (shell) spaces. The lumens are open along the tube sheet. Upon sealing the tube sheet to the case, separate manifolds on the case exterior allow the introduction and removal of fluid streams to the lumen and shell spaces. The feed can be introduced to either the lumen or shell. A permeate sweep also may be fed to the module. The sweep mixes with the permeate and can improve the module

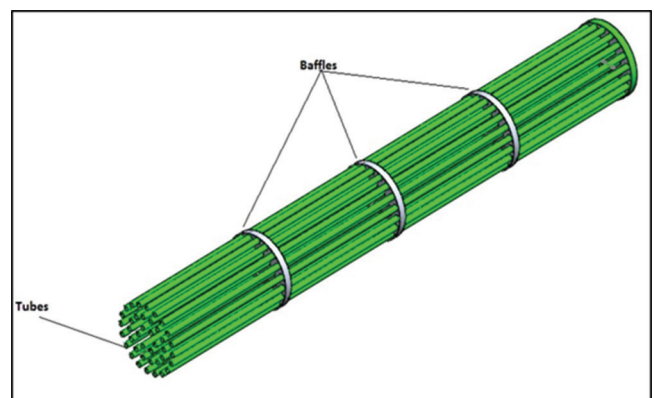


Fig. 1. 3D drawing of bundle of hollow fiber membrane distillation with supporting baffles.

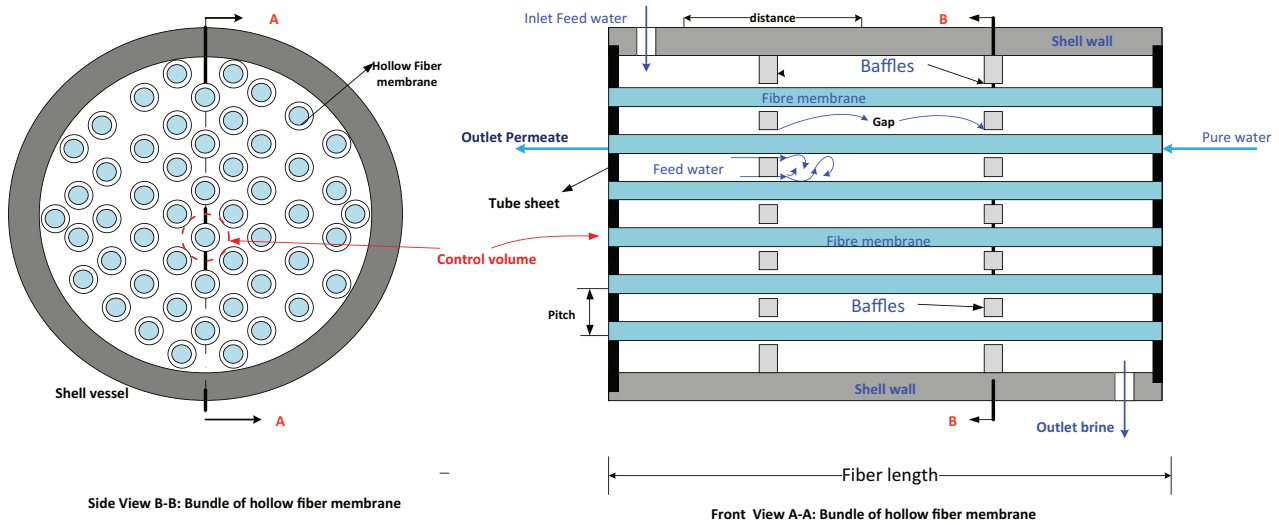


Fig. 2. Module of hollow fiber membrane arrangement with supporting baffles.

performance by creating potential vapor pressure difference across membrane.

The baffle is used as tube support in order to prevent clustering of the fiber. This bundle of fibers passes through the baffles and is enclosed in the shell (vessel). The horizontal distance between baffles is considered as design parameter which needs to be evaluated and investigated its impact on the membrane distillation module performance. The distance between fibers functions as the fiber diameter which is defined by pitch which varies from 1.25 to 2. The packing density which represents the volume of fibers to the volume of enclosed shell vessel is needed to be evaluated and investigated its impact on mass and heat transfer and pressure drop within module. In order to facilitate the hot seawater flow within shell side annular gap around each fiber is designed in the tube support as shown in Fig. 2. The annular gap (clearance) between fiber and the baffle sheet is designed to facilitate the flow of seawater feed and to create high turbulence flow in order to improve the mass flux through. A number of baffles are distributed in equal distance along the module length in order to support the fibers inside the shell. The hot seawater feed is directed to the shell side at the left end of the vessel while the pure water is passed through the inner diameter of the fibers countercurrent flow. The shell vessel length is designed as 1 m length which is the same length of the fibers. The flow in the shell side assumed uniform and parallel to the fiber length. The pitch between fibers is a function of the fiber outside diameter (D). It is assumed that the height of the gap around the fiber is symmetrically aligned with gap center.

2.2. Computational domain and boundary conditions

The overall governing transport equations for the feed, the permeate, local mass flux, thermal efficiency convection heat transfer, temperature polarization, local Reynolds number and hydraulic energy consumption are illustrated in the Appendix 1. Fig. 3 shows the boundary conditions of a single hollow fiber with baffle modules. Uniform velocity and temperature are specified at the entrance of the feed and permeate sides.

A baseline for process performance can be determined by assuming the fibers are uniform (identical inner and outer radii) and uniformly spaced. Additionally, baseline performance predictions assume the fluid distribution is uniform from the external ports on the case through the manifolds to the lumen and shell. The performance of this “ideal” device can be determined by analyzing the performance of a single fiber. The low feed velocity is specified as 0.06 m s^{-1} (laminar flow, $Re_f = 836$), while the permeate velocity is specified as 0.42 m s^{-1} (laminar flow, $Re_p = 460$). The hot feed temperature varies from 327 to 337 K, while the inlet permeate temperature is fixed at 294 K. The outlet pressure is specified as atmospheric pressure.

The properties of the polymeric membrane can be expressed as follows:

$$\phi m = \phi_{ms} (1 - \epsilon) + \epsilon \phi_{mg} \quad (1)$$

where general variable symbols, ϕ_{ms} and ϕ_{mg} , are the properties (density, specific heat and thermal conductivity) of the membrane material and vapor, respectively, ϵ is the porosity of the membrane. In the present study, hydrophobic polyvinylidene fluoride (PVDF) membrane porosity, 0.83, was used [12]. Other relevant testing fluids and properties of the PVDF hollow fiber membrane are listed in Tables 1 and 2, respectively. The specifications of the PVDF hollow fibers and modules are listed in Table 3.

In order to optimize the grid structure, in the radial direction a grid scale of $5 \times 10^{-6} \text{ m}$ is chosen for the bulk permeate and membrane. The triangular grid is chosen for the bulk feed (shell side); while in the axial direction a universal grid scale of $1 \times 10^{-4} \text{ m}$ is employed. The 2D grid configuration along fiber length is shown in Fig. 3. In the current membrane distillation system, the effect of the hollow fiber membrane surface roughness on the wall boundary conditions is ignored as it has a magnitude of 10^{-8} m , which is far smaller than the grid scale. The simulation is carried out using ANSYS Fluent 14.5, with SIMPLE (semi-implicit method for pressure linked equations) algorithm for pressure–velocity coupling and QUICK (quadratic upstream interpolation for convective kinetics) algorithm for discretization of the conservation

Table 1
Properties of the fluids [17]

Material	Density (kg m^{-3})	Specific heat ($\text{J kg}^{-1} \text{K}^{-1}$)	Thermal conductivity ($\text{W m}^{-1} \text{K}^{-1}$)	Viscosity $\times 10^{-4} \text{ Pa s}$
3.5% seawater (323 K)	1,013.2	4,064.8	0.642	5.86
Pure water (303 K)	995.2	4,182.1	0.613	8.38

Table 2
Properties of the PVDF membrane [12]

Material	Density (kg m^{-3})	Specific heat ($\text{J kg}^{-1} \text{K}^{-1}$)	Thermal conductivity ($\text{W m}^{-1} \text{K}^{-1}$)
PVDF	1,775	1,325	0.2622
Vapor*	0.554	2,014	0.0261
Membrane	302.2	1,896.9	0.0662

*Properties of vapor obtain from the database of ANSYS Fluent 14.5.

Table 3
PVDF membrane properties and module specification

Membrane properties			Module specifications	
Material	Dimension	Porosity ε (%)	Shell diameter $d_s = 100 \text{ mm}$	No. of fibers N 977, 1,211, 1,639, 2,563
PVDF	Ro: 0.725 mm δ_m : 275 μm	83	Effective fiber length $L = 1 \text{ m}$	Packing density 20%, 25%, 35%, 50%

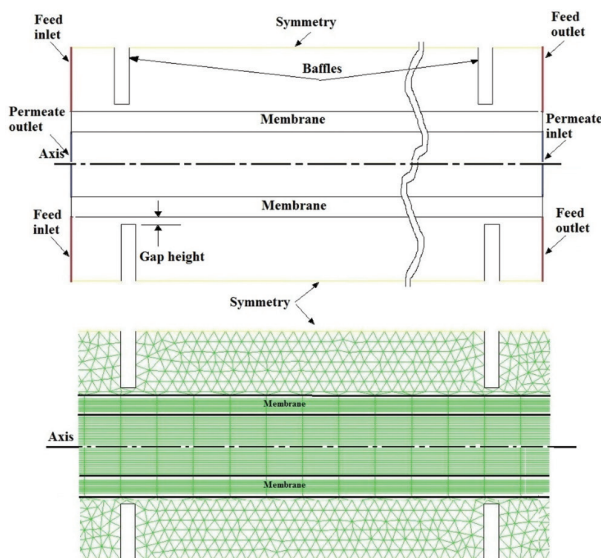


Fig. 3. CFD domain of single fiber in 2D and mesh generation.

equations. Interpolation for convective kinetics algorithm is used for discretization of the conservation equations. The convergence criterion of 10^{-6} was chosen for convergence. Based on the above operating conditions, a laminar model was applied to the conservation equations for the traditional module; while in a modified configuration, a realizable $k-\varepsilon$ model with enhanced wall treatment is employed to simulate the turbulence induced by the introduction of baffles.

3. Results and discussion

3.1. Model validation

The presented CFD model is validated using experimental and simulation results of single fiber of 0.25-m-long hollow fiber published in [12]. The comparison is performed under the same operating and design conditions illustrated in Tables 1–3. Fig. 4 shows the distribution of the local mass flux along the fiber length for the present model and the referenced results [12]. The simulation data are in good agreement with the reference model since the maximum deviation of 1% is noted between the current model and the reference model. Fig. 5 shows TPC distribution along the fiber that varies between 0.68 and 0.7 for present work and reference data of [12], respectively. A maximum deviation between the two models is calculated to be around 2%.

3.2. The effect of baffle orientation

Fig. 6(a) shows the velocity distribution on the feed side of the membrane fiber at different gap heights (0.05, 0.075 and 0.1 mm). This figure, also, shows that by decreasing the gap height, the velocity through the gap increases which creates eddy streams on the back side of the baffle. This is due to high water velocity through the gap and the sudden enlargement. These eddy streams create turbulence in the downstream of the baffle which reduce the thermal boundary layer around the fiber and improve the mass flux. Fig. 6(b) illustrates the CFD simulation results of a typical pressure distribution along a single fiber with baffle at different gap height

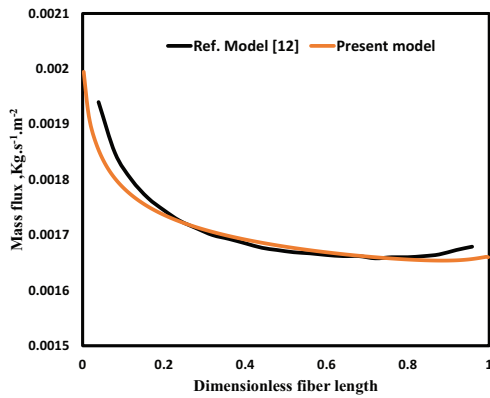


Fig. 4. The distributions of local mass flux along the fiber length (L = 0.25 m).

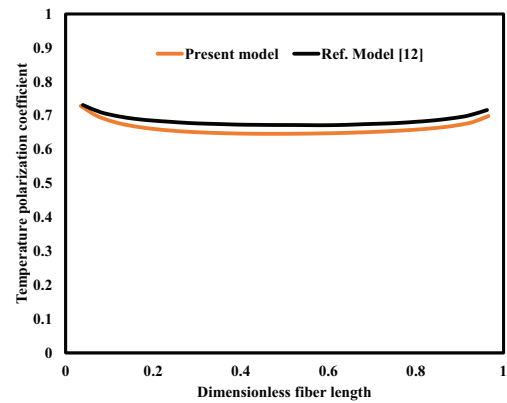


Fig. 5. TPC distributions along the fiber length (L = 0.25 m).

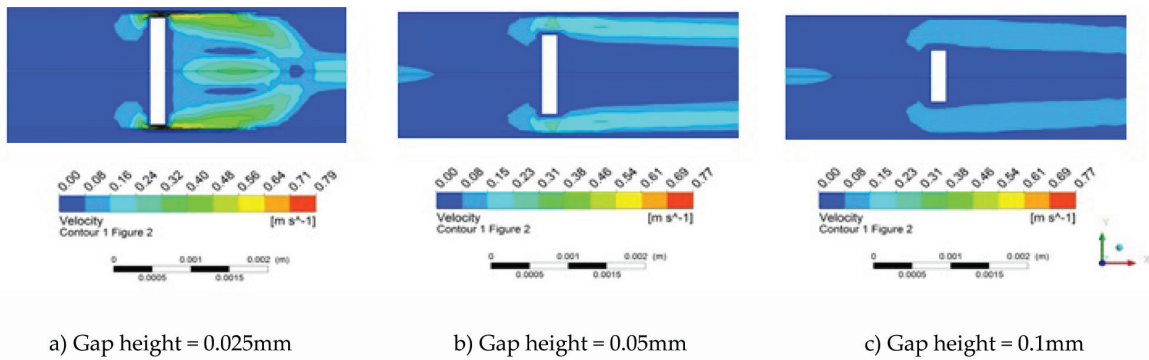


Fig. 6(a). Velocity contour at various gap height ($\phi = 1.25D$, $C = 2 \times 10^{-7} \text{ kg m}^{-2} \text{ s}^{-1} \text{ Pa}^{-1}$, $L = 1 \text{ m}$).

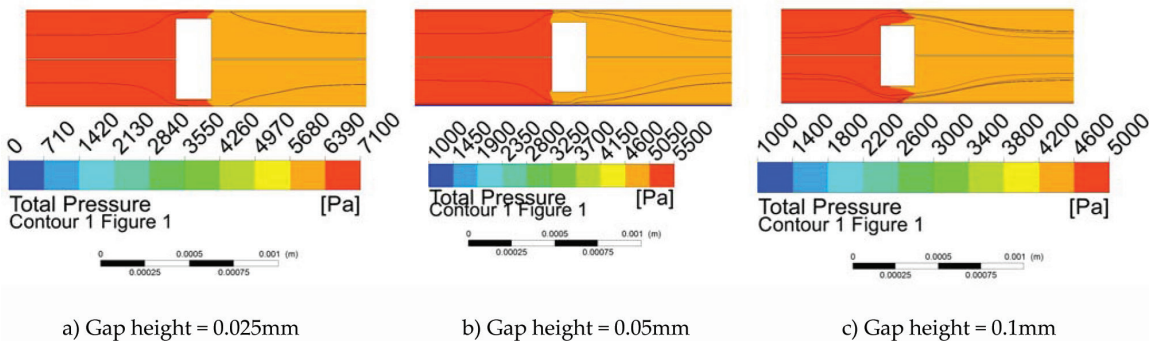


Fig. 6(b). Pressure distribution at different gap height ($\phi = 1.25D$, $C = 2 \times 10^{-7} \text{ kg m}^{-2} \text{ s}^{-1} \text{ Pa}^{-1}$, $L = 1 \text{ m}$).

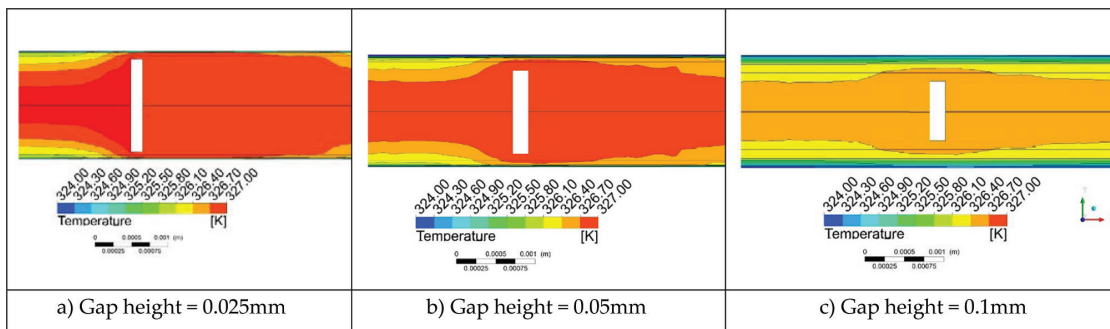


Fig. 6(c). Temperature distribution at different gap height ($\phi = 1.25D$, $C = 2 \times 10^{-7} \text{ kg m}^{-2} \text{ s}^{-1} \text{ Pa}^{-1}$, $L = 1 \text{ m}$).

(0.05, 0.075 and 0.1 mm). The results show that comparatively high pressure drop occurs across the baffle because of the flow contraction occurs through small gap height. Fig. 6(c) shows temperature distribution at different gap height (0.05, 0.075 and 0.1 mm) in the vicinity of the hollow fiber wall. Gradient in temperature is notable in the region that far away baffle which reflect the thermal boundary layer resistance. However, at the baffle gap, the temperature gradient is very small to notice which indicates the baffle gap suppresses the thermal boundary layer resistance which would improve the mass transfer of membrane distillation process.

Fig. 7 shows the local velocity distribution in the feed side where eight baffles are allocated along a meter-length fiber at equal distances and the gap height is maintained as 0.075 mm. The velocity profile peak is occurring at the baffle due to the small gap between the inner diameter of the baffle and the outer diameter of the fiber. However, the fluid velocity tends to recover and regain its original momentum after passing through the baffle. It can also be seen that the fluid flow remains laminar ($Re_f = 836$) adjacent to the wall before reaching the baffle where the flow velocity is at its normal value. The presence of an array of baffles not only increases turbulence in the bulk fluid stream as shown in Fig. 6(a) but also interrupts the build-up of boundary layer formation on the membrane surface as well as prevents the particles suspended in the feed, which are more prone to deposit on the membrane surface that may adversely decline the permeation flux.

Fig. 8 shows Reynolds number feed flow variation along the module length where eight baffles are allocated along a meter-length fiber at equal distances and the gap height is maintained as 0.075 mm. The Reynolds number peak occurs at the gap which is explained by high flow velocity through the gap as shown in Fig. 7.

Fig. 9 shows the distribution of feed side pressure drop along membrane fiber. A sudden drop in the local pressure would occur at the gap as a result of the friction and the eddy formation. The amount of pressure drop along the length of the module can be determined from the difference in total pressure between the inlet ($x = 0$ m) and outlet ($x = 1$ m) which is calculated in the order of 5 kPa.

Fig. 10 shows that the simulated convection heat transfer

coefficient in the feed side. The peaks values of the convection heat transfer coefficient occur at gaps are due to existence of the turbulence flow. The average convection heat transfer coefficient of the baffled module is 30% higher than that of the original module. This significant improvement in heat-transfer coefficients is achieved by introducing the baffle which suppresses the build-up of the boundary layers consequently decreasing the thermal polarization effect.

Fig. 11 shows that the average values of the vapor mass flux increase with decreased gap height. This is mainly due to reduction in the thermal boundary layer thickness. The mass flux reaches its peak at gap height of 0.025 mm compared with the original module (without baffle). The mass flux for both the original and the baffled module decreases along the fiber length. This is due to low thickness of the thermal boundary layer at the entrance region comparatively to the progressively increases until it reaches the fiber outlet.

Fig. 12 shows that the average thermal efficiencies (η_{th}) increases as the gap height decreases. The average thermal efficiency η_{th} varies from 0.35 to 0.55 when the gap height decreases from 0.1 to 0.025 mm. The enhancement in average thermal efficiency is calculated to be 12% at gap height = 0.1 mm and 22% at gap height = 0.025 mm.

Fig. 13 shows that the mass flux increases with increasing numbers of baffles. This is due to formation of extended turbulent flow zones which are created by the baffles. Fig. 13 also shows that the potential improvement in the mass flux loses its impact when the number of baffles becomes greater than eight, as turbulence in the module also reaches its peak.

Fig. 14 shows the effect of the number of the baffles on the temperature polarization coefficient (TPC) at gap height of 0.075 mm. The noticeable increase in the local TPC occurs at gaps. This is mainly due to the reduction in the thickness of thermal layer at the baffle. The average value of the TPC along the fiber length in the baffle module is 16% higher than that of the original module.

Fig. 15 shows the required specific hydraulic energy consumption (SHEC) at different number of baffles to push the water feed through the shell side. This figure shows that the required pumping power increases as the number of baffles increase. Also, the SHEC increases as the gap height decreases. This is mainly due to increase in the pressure drop

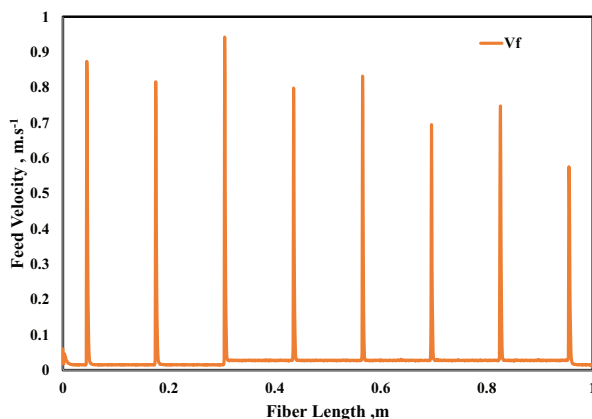


Fig. 7. Feed velocity distribution along module fiber length (gap = 0.075 mm).

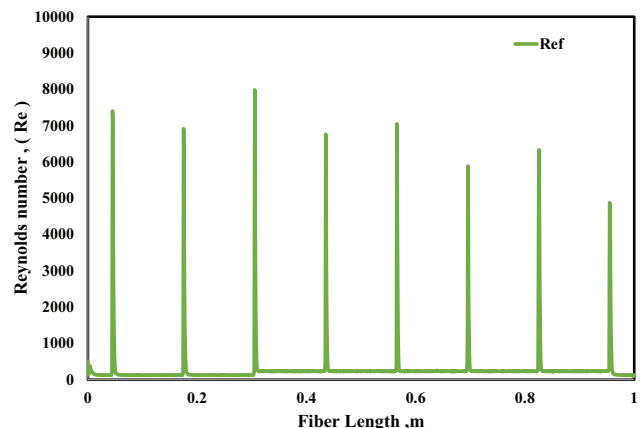


Fig. 8. Reynolds number of feed flow along module length (gap = 0.075 mm).

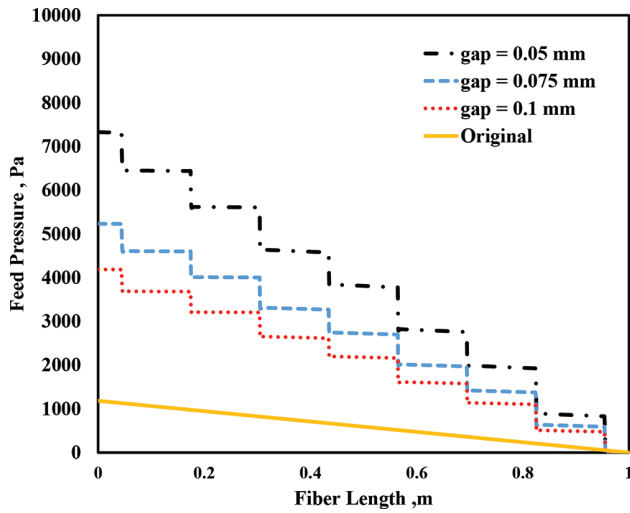


Fig. 9. Feed pressure distribution along module fiber length (eight baffles).

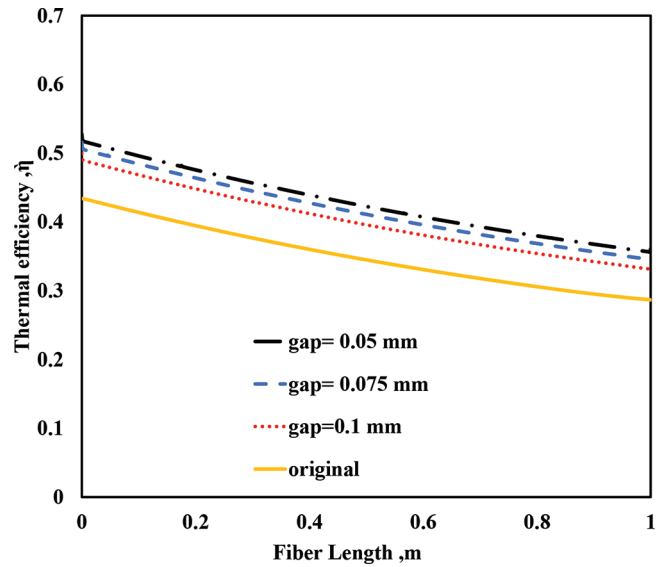


Fig. 12. Thermal efficiency distribution along the fiber length (eight baffles).

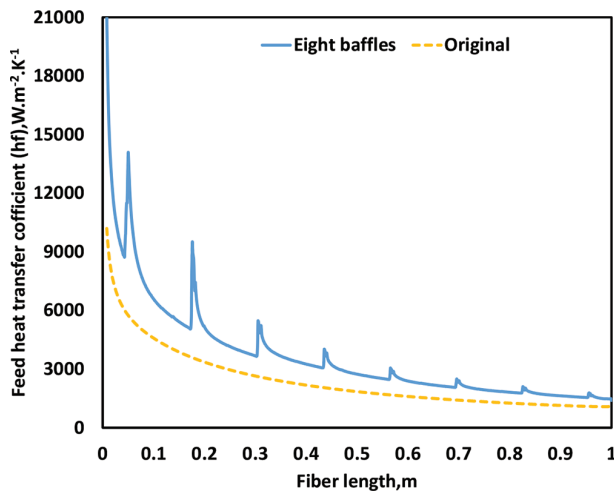


Fig. 10. Convection heat transfer coefficient variation along the module length (gap = 0.075 mm).

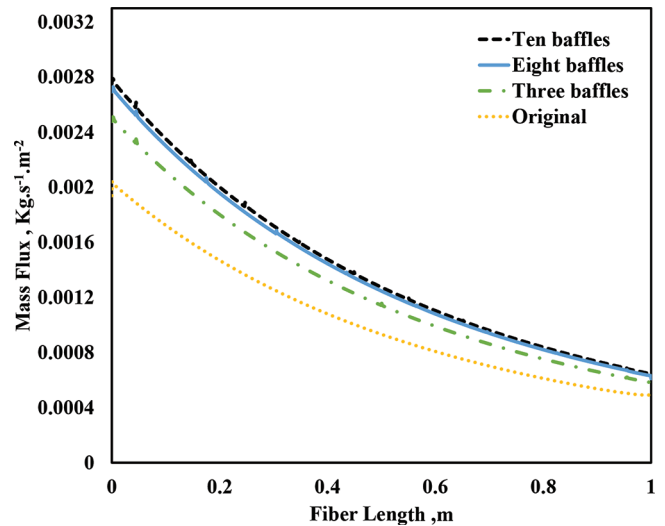


Fig. 13. The mass flux variation at different number of baffles (gap = 0.075 mm).

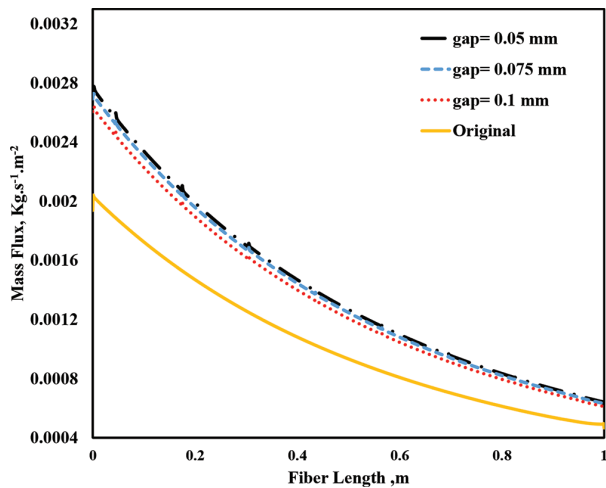


Fig. 11. Mass flux variation at various gap heights (eight baffles).

across baffle as a result of high velocity flow passing through the gaps.

3.3. Effect of packed density

The packing density of membrane fibers when it is installed as the bundle in 4-inch vessel varies from 20% to 50% according to the pitch variation as shown in Table 4. The number of packed fibers is calculated as 977, 1,211, 1,639 and 2,563 at pitches of 2D, 1.75D, 1.5D and 1.25D, respectively. Accordingly, the total calculated surface area of the fibers in the vessel is 4.5, 5.5, 7.5 and 11.7 m².

Fig. 16 shows that the module water production increases as the pitch decreases (high packing density). This is mainly due to higher surface area of the membrane as well as the

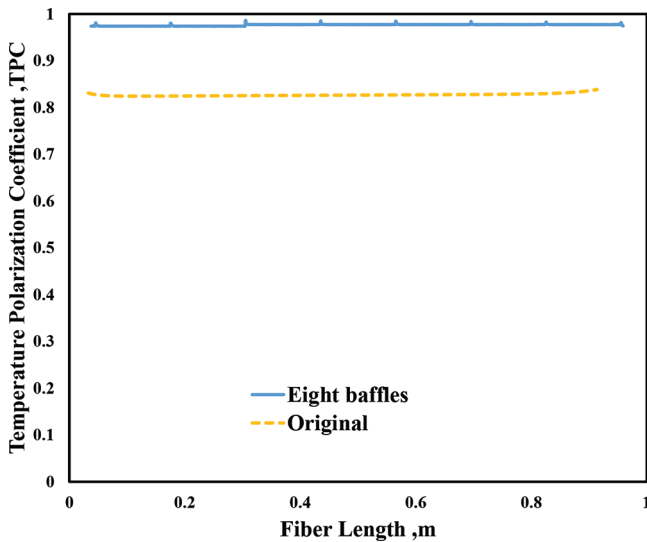


Fig. 14. The TPC distribution along the module length (gap = 0.075 mm).

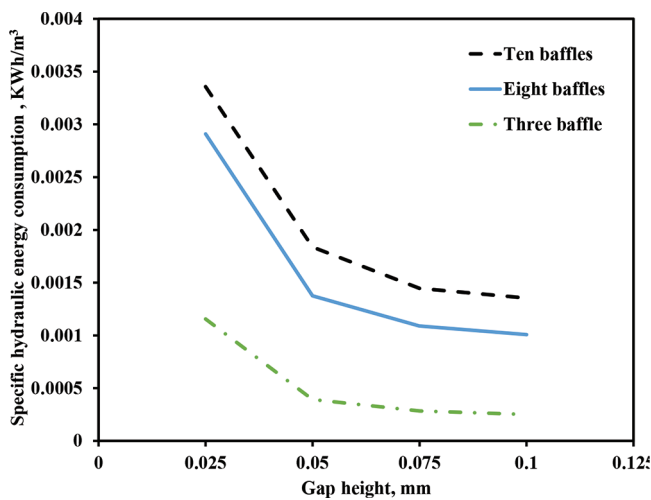


Fig. 15. The effect of various gaps and numbers of baffles on SHEC.

high water velocity created around fibers. The water production rate for eight baffles module with 1.25D pitch (50% packing density), and gap height of 0.075 mm is 25% higher than that of the original module.

Fig. 17 shows that the hydraulic energy consumption in the baffle module is relatively higher at small pitches. This is mainly due to increase in the friction pressure drop that occurs at high velocity through the gap. At packing density of 50% (pitch = 1.25D) and gap height of 0.075 mm, the specific energy consumption of the baffle module is 21% higher than the original module.

Figs. 16 and 17 show that the small pitch (i.e., high packing density) is recommended from the module production point of view; however, the high packing density configuration encounters high pressure drop within the module. Therefore, a compromise between high module production and acceptable specific energy consumption is the governing factor that needs to be balanced on a case-by-case basis. The trade-off between performance enhancement and hydraulic energy consumption is compromised and determined at 1.25D pitch, eight baffle supports and at a gap height of 0.075 mm.

4. Conclusions

A new baffle is proposed to enhance the local mass flux and thermal efficiency of the hollow fiber membrane distillation. The baffles are designed to assemble a bundle of hollow fibers to prevent fiber clustering and to structurally support the bundle of fibers. They are also used as a diffuser turbulence promoter. Using CFD analysis, the contribution of the baffle sheet is summarized as follows:

- The average mass flux is 25% higher than that of the original module.
- The average TPC is 16% higher than that of the original modules.
- The average thermal efficiency (η) is 16% higher than the original module.
- The water production rate per module is 25% higher than that of the original module.

High packing density module is recommended from the module production point of view; however, the high

Table 4
Packed density variation

Pitch (ϕ)	1.25 D	1.5 D	1.75 D	2 D
No. of fiber	$N = 2,563$	$N = 1,639$	$N = 1,211$	$N = 977$
Packed density	50%	35%	25%	20%

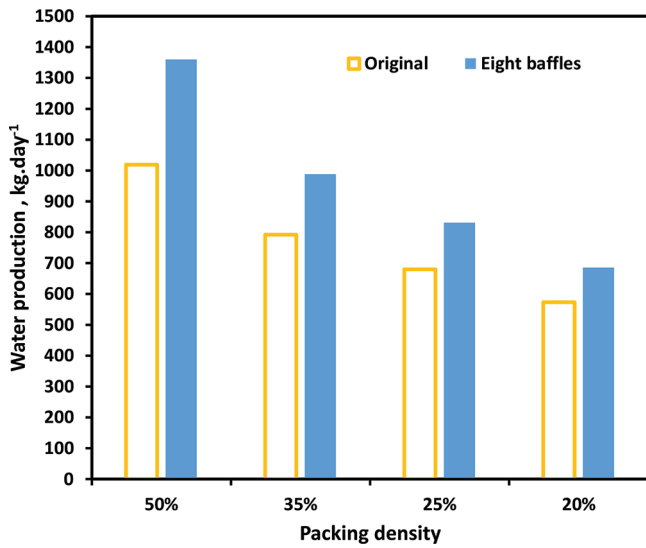


Fig. 16. Water production at different pitch (packing density) (gap = 0.075 mm).

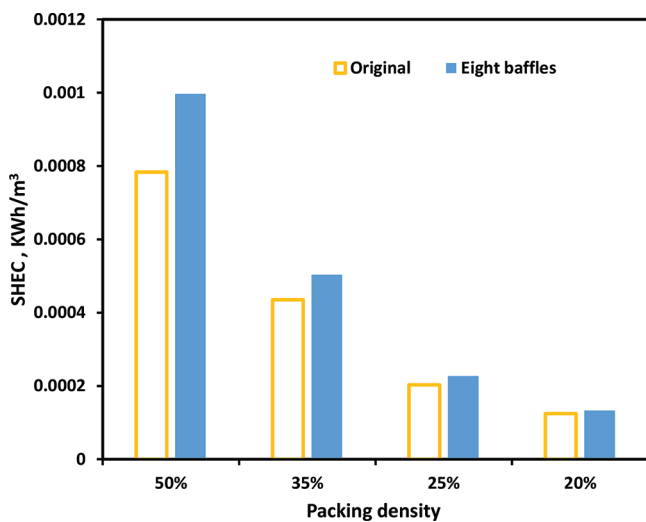


Fig. 17. Specific hydraulic energy consumption at different pitch (packing density) (gap = 0.075 mm).

packing density configuration encounters higher pressure drop. Therefore, a compromise between high packing density module (high production) and acceptable specific pumping energy consumption is the governing factor that needs to be balanced on a case-by-case basis. The trade-off between performance enhancement and hydraulic energy consumption is compromised and determined at 1.25D pitch (50% packing density), eight baffle supports and at a gap height of 0.075 mm.

Nomenclature

- A — Membrane area, m²
- C — Mass transfer coefficient of the membrane, kg m⁻²s⁻¹Pa⁻¹

- C_p — Specific heat capacity of material, J kg⁻¹K⁻¹
- D — Hollow fiber outer diameter, m
- d — Hollow fiber inner diameter, m
- h — Heat transfer coefficient of fluid, W m⁻²K⁻¹
- SHEC — Specific hydraulic energy consumption, J kg⁻¹
- k — Thermal conductivity, W m⁻¹K⁻¹
- L — Length of module or hollow fiber, m
- LH_T — Latent heat of vaporization of water, J kg⁻¹
- Nm — Transmembrane mass flux, kg m⁻²s⁻¹
- Nu — Nusselt number
- P — Water vapor pressure, Pa
- Pr — Prandtl number
- q — Heat flux, W m⁻²
- Re — Reynolds number
- R_{mi} — Inner radii of hollow fiber
- R_{mo} — Outer radii of hollow fiber, m
- S_h — Source term of energy transport equation, J m⁻³s⁻¹
- v — Velocity of feed or permeate, m s⁻¹
- V — Volume flow rate, m³/sec
- x, r — Axial, radial direction in cylindrical coordinate, m

Greek symbols

- η_h — Thermal efficiency
- μ — Viscosity, Pa s
- ρ — Density, kg m⁻³
- ϵ — Membrane porosity, %
- δ_m — Membrane thickness, μ m

Subscripts

- b — Bulk average value
- f — Feed
- fi, fo — Entrance, outlet of feed
- fm — On feed-side membrane surface
- m — Membrane, or membrane surface
- p — Permeate
- pi, po — Entrance, outlet of permeate
- pm — On permeate-side membrane surface

References

- [1] J.I. Mengual, M. Khayet, M.P. Godino, Heat and mass transfer in vacuum membrane distillation, *Int. J. Heat Mass Transfer*, 47 (2004) 865–875.
- [2] M. Khayet, T. Matsuura, *Membrane distillation: principles and applications*, Elsevier (2011).
- [3] M.J. Costello, A.G. Fane, P.A. Hogan, R.W. Schofield, The effect of shell side hydrodynamics on the performance of axial flow hollow fiber modules, *J. Membr. Sci.*, 80 (1993)1–11.
- [4] N.C. Mat, Y. Lou, G.G. Lipscomb, Hollow fiber membrane modules, *Curr. Opin. Chem. Eng.*, 4 (2014) 18–24.
- [5] K. Charfi, M. Khayet, M.J. Safi, Numerical simulation and experimental studies on heat and mass transfer using sweeping gas membrane distillation, *Desalination*, 259 (2010) 84–96.
- [6] G.A. Weihs, D.E. Wiley, Review of 3D CFD modeling of flow and mass transfer in narrow spacer-filled channels in membrane modules. *Chem. Eng. Process.: Process Intensification*, 49 (2010) 759–781.
- [7] H. Yu, X. Yang, R. Wang, A.G. Fane, Analysis of heat and mass transfer by CFD for performance enhancement in direct contact membrane distillation, *J. Membr. Sci.*, 405 (2012) 38–47.
- [8] X. Yang, H. Yu, R. Wang, A.G. Fane, Analysis of the effect of turbulence promoters in hollow fiber membrane distillation modules by computational fluid dynamic (CFD) simulations, *J. Membr. Sci.*, 415 (2012) 758–769.

- [9] M.M. Teoh, S. Bonyadi, T.S. Chung, Investigation of different hollow fiber module designs for flux enhancement in the membrane distillation process, *J. Membr. Sci.*, 311 (2008) 371–379.
- [10] M. Shakaib, S.M.F. Hasani, I. Ahmed, R.M. Yunus, A CFD study on the effect of spacer orientation on temperature polarization in membrane distillation modules, *Desalination*, 284 (2012) 332–340.
- [11] X. Yang, R. Wang, A.G. Fane, Novel designs for improving the performance of hollow fiber membrane distillation modules, *J. Membr. Sci.*, 384 (2011) 52–62.
- [12] H. Yu, X. Yang, R. Wang, A.G. Fane, Numerical simulation of heat and mass transfer in direct membrane distillation in a hollow fiber module with laminar flow, *J. Membr. Sci.*, 384 (2011) 107–116.
- [13] T.E. Graham, Hollow Fiber Permeator, US Patent 4,367,139 (1983) 22.
- [14] T.L. Caske, J.L. Trimmer, J.L. Jorgensen, Hollow Fiber Membrane Fluid Separation Module for Boreside Feed, US Patent 4,929,259 (1990).
- [15] M.M. Shirazi, A. Kargari, M.J.A. Shirazi, Direct contact membrane distillation for seawater desalination, *Desalin. Water Treat.*, 49 (2012) 368–375.
- [16] C.Y. Iguchi, W.N.D. Santos, R. Gregorio, Determination of thermal properties of pyro electric polymers, copolymers and blends by the laser flash technique, *Polym. test.*, 26 (2007) 788–792.
- [17] K. He, H.J. Hwang, M.W. Woo, I.S. Moon, Production of drinking water from saline water by direct contact membrane distillation (DCMD), *J. Ind. Eng. Chem.*, 17 (2011) 41–48.
- [18] A.O. Imdakm, T. Matsuura, Simulation of heat and mass transfer in direct contact membrane distillation (MD): the effect of membrane physical properties, *J. Membr. Sci.*, 262 (2005) 117–128.
- [19] B.S. Sparrow, Empirical equations for the thermodynamic properties of aqueous sodium chloride, *Desalination*, 159 (2003) 161–170.
- [20] R.W. Schofield, A.G. Fane, C.J.D. Fell, Heat and mass transfer in membrane distillation, *J. Membr. Sci.*, 33 (1987) 299–313.

Appendix 1

Mathematical model

A. Governing transport equations

The overall governing transport equations for the feed permeate and membrane, local mass flux, convection heat transfer, temperature polarization, local Reynolds number, and hydraulic energy consumption are as follows [3, 4, 12]:

The continuity equation:

$$\nabla \cdot (\rho \cdot \vec{v}) = 0 \quad (1)$$

The momentum transport equation:

$$\nabla \cdot (\rho \vec{v} \vec{v}) = \nabla \rho + \nabla \cdot (\vec{\tau}) + \rho \vec{g} \quad (2)$$

where $\vec{\tau}$ is the stress tensor, which can be expressed as follows:

$$\vec{\tau} = \mu \left[\nabla \vec{v} + \nabla \vec{v}^T \right] - \frac{2}{3} \nabla \cdot \vec{v} I \quad (3)$$

The energy conservation equation:

$$\nabla \cdot (\rho \vec{v} C_p T) = \nabla \cdot (k \nabla T) + S_n \quad (4)$$

where k is the heat conductivity; S_n is the heat-source term for the feed or permeate on the membrane surface, and indicates the amount of latent heat generated by evaporation at the hot side membrane surface and subsequently released through condensation at the cold-side membrane surface. It can be written as follows:

$$S_n = \frac{q_{MD}}{\delta r} \rightarrow r = R_{mi} \quad \text{and} \quad S_n = \frac{q_{MD}}{\delta r} \rightarrow r = R_{mo} \quad (5)$$

where q_{MD} is the heat flux on the feed side membrane surface; r is the radial direction; δr is the chosen grid thickness in the r direction. R_{mi} and R_{mo} are the inner and outer radial of the fiber, respectively.

At membrane wall: no-slip condition, conjugate heat conduction:

$$\begin{aligned} q_f |_{R_{mo}} &= q_m |_{R_{mo}}, \quad q_m |_{R_{mi}} = q_p |_{R_{mi}} \\ T_f |_{R_{mo}} &= T_m |_{R_{mo}}, \quad T_m |_{R_{mi}} = T_p |_{R_{mi}} \end{aligned} \quad (6)$$

B. Mass and heat transfer

The local transmembrane mass flux N_m is calculated by the simplest form of vapor flux, which is given as a linear function of vapor pressure difference across the membrane such as [15–20]:

$$Nm = C \frac{dP}{dT} (T_{mf} - T_{mp}) \quad (7)$$

where the gradient dp/dT is given by Antoine equation:

$$\frac{dP}{dT} = 3841 \frac{\exp\left(23.238 - \frac{3841}{T_m - 45}\right)}{(T_m - 45)^2} \quad (8)$$

where C is the mass transfer coefficient of the membrane, which is equal to $2.0 \times 10^{-7} \text{ kg m}^{-2} \text{ s}^{-1} \text{ Pa}^{-1}$.

The saturated vapor pressure at the membrane interface temperature is calculated from the Antoine equation [18]:

$$P = \exp\left(23.238 - \frac{3841}{T_m - 45}\right) \quad (9)$$

where $T_m = (T_{bf} + T_{bp})/2$.

The heat transfer across the liquid films (feed side q_f or permeate side q_p) can be expressed as [12]:

$$q_f = q_p \quad (10)$$

$$q_f = h_f \Delta T_f = h_f (T_{bf} - T_{mf}) \quad (11)$$

$$q_p = h_p \Delta T_p = h_p (T_{mp} - T_{bp}) \quad (12)$$

where h_f and h_p can be calculated using Eqs. (11) and (12) based on membrane wall temperatures T_{mf} , T_{mp} and average bulk temperature for feed and permeate T_{bf} and T_{bp} , respectively.

The total heat transport in membrane distillation consists of conductive heat through the membrane and the latent heat contributing to the vapor flux [12]:

$$q_{MD} = q_c + q_v = h_m (T_{mf} - T_{mp}) + N_m \cdot LH_{Tmf} \quad (13)$$

The h_m is the heat transfer coefficient of the hydrophobic membrane, which can be calculated from the thermal conductivities of the hydrophobic membrane polymer (k_{ms}) and the thermal conductivity coefficients of vapor within the membrane pore (k_{mg}).

$$h_m = \frac{K_m}{R_{mi} \cdot 1n \left(\frac{R_{mo}}{R_{mi}} \right)} = \frac{K_{mg} \varepsilon + K_{ms} (1 - \varepsilon)}{R_{mi} \cdot 1n \left(\frac{R_{mo}}{R_{mi}} \right)} \quad (14)$$

where ε and k_m are the membrane porosity and thermal conductivity of the hydrophobic membrane, respectively.

Where LH_{Tmf} , LH_{Tmi} is the latent heat of evaporation ($J \text{ kg}^{-1}$), which is calculated as follows [17]:

$$LH_{Tmf} = 2501.897149 - 2.407064037 T_{mf} + 0.001192217 T_{mf}^2 - 0.000015863 T_{mf}^3 \quad (15)$$

where T_{mf} , temperature in °C.

The temperature polarization coefficient (TPC) is defined as the ratio between the actual driving force and the theoretical driving force [18–20]; as a result the TPC is expressed mathematically as follows:

$$TPC = \frac{T_{mf} - T_{mp}}{T_{bf} - T_{bp}} \quad (16)$$

The thermal efficiency η_{th} is the fraction of the heat transfer that contributes to the evaporation [6]:

$$\eta_{th} = \frac{N_m \cdot LH_{Tfm}}{Q_f} = \frac{N_m \cdot LH_{Tfm}}{N_m \cdot LH_{Tfm} + h_m (T_{fm} - T_{pm}) dm / do} \quad (17)$$

C. The hydraulic energy consumption (HEC)

To fully evaluate these fibers of various geometries, two important process metrics, water production ($\text{kg} \cdot \text{day}^{-1}$) and hydraulic energy consumption (HEC), were calculated and compared among various modules.

The Reynolds number is calculated as follows:

$$R_{ef} = \frac{\rho_f v_f D_{eq}}{\mu_f} \quad (18)$$

$$D_{eq} = \frac{4 \left[\frac{P_t}{2} (0.86 P_t) - \frac{1}{2} \frac{\pi D^2}{4} \right]}{\pi D} \quad (19)$$

where P_t , tube pitch, D , tube fiber outside diameter. R_{ep} , T_{fi} and T_{bi} are Reynolds number and inlet bulk temperature of feed and permeate, respectively. The term, v_f (feed velocity), is obtained from CFD simulations.

$$HEC = \frac{\Delta p \times v}{N_m \times A} \quad (20)$$

where A is the total membrane area of fibers, V is the volume flow rate m^3/sec , and Δp is the differential pressure between feed inlet and outlet.